Journal of Molecular Structure 1119 (2016) 139–150

Contents lists available at ScienceDirect

Journal of Molecular Structure

journal homepage: http://www.elsevier.com/locate/molstruc

Thiazole-based nitrogen mustards: Design, synthesis, spectroscopic studies, DFT calculation, molecular docking, and antiproliferative activity against selected human cancer cell lines

Krzysztof Z. Łączkowski [a, *], Marta Świtalska [b], Angelika Baranowska-Łączkowska [c], Tomasz Plech [d], Agata Paneth [d], Konrad Misiura [a], Joanna Wietrzyk [b], Barbara Czaplińska [e], Anna Mrozek-Wilczkiewicz [f, g], Katarzyna Malarz [e], Robert Musioł [e], Izabela Grela [h]

[a] Department of Chemical Technology and Pharmaceuticals, Faculty of Pharmacy, Collegium Medicum, Nicolaus Copernicus University, Jurasza 2, 85-089, Bydgoszcz, Poland
[b] Institute of Immunology and Experimental Therapy, Polish Academy of Sciences, Rudolfa Weigla 12, 53-114, Wrocław, Poland
[c] Institute of Physics, Kazimierz Wielki University, Plac Weyssenhoffa 11, 85-072, Bydgoszcz, Poland
[d] Department of Organic Chemistry, Faculty of Pharmacy, Medical University, Chodźki 4a, 20-093, Lublin, Poland
[e] Institute of Chemistry, University of Silesia, Szkolna 9, 40-006, Katowice, Poland
[f] A. Chełkowski Institute of Physics, University of Silesia, Uniwersytecka 4, Katowice, 40-007, Poland
[g] Silesian Center for Education and Interdisciplinary Research, 75 Pulku Piechoty 1A, Chorzów, 41-500, Poland
[h] Faculty of Chemical Technology and Engineering, University of Technology and Life Sciences, Seminaryjna 3, 85-326, Bydgoszcz, Poland

ARTICLE INFO

Article history:
Received 12 March 2016
Received in revised form
18 April 2016
Accepted 19 April 2016
Available online 27 April 2016

Keywords:
Antiproliferative activity
Thiazole
Nitrogen mustard
DFT calculations
Nucleobases
Topoisomerase

ABSTRACT

Synthesis, characterization and investigation of antiproliferative activity of ten thiazole-based nitrogen mustard against human cancer cells lines (MV4-11, A549, MCF-7 and HCT116) and normal mouse fibroblast (BALB/3T3) is presented. The structures of novel compounds were determined using ^{1}H and ^{13}C NMR, FAB(+)-MS, and elemental analyses. Among the derivatives, **5b**, **5c**, **5e**, **5f** and **5i** were found to exhibit high activity against human leukaemia MV4-11 cells with IC_{50} values of 2.17–4.26 μg/ml. The cytotoxic activity of compound **5c** and **5f** against BALB/3T3 cells is up to 20 times lower than against cancer cell lines. Our results also show that compounds **5e** and **5i** have very strong activity against MCF-7 and HCT116 with IC_{50} values of 3.02–4.13 μg/ml. Moreover, spectroscopic characterization and cellular localization for selected compound were performed. In order to identify potential drug targets we perform computer simulations with DNA-binding site of hTopoI and hTopoII and quantum chemical calculation of interaction and binding energies in complexes of the five most active compounds with guanine.

1. Introduction

Cancer is one of the most significant health problems of modern civilization [1]. It is the major cause of death, and according to the WHO report it is estimated that 14.1 million new cancer cases and 8.2 million cancer-related deaths occurred in 2012. The highest incidence of cancer is observed in rapidly developing countries and it is estimated that the number of new cancer cases per year will further increase to 19.3 million by 2025 [2].

DNA alkylating agents with the nitrogen mustards remain an important group in the modern anti-cancer drug development and therapy [3]. The preferential site in DNA alkylation depends on the nature of alkylating agents and occurs mostly on position N7 and O6 in guanine, N1 and N3 in adenine, and N3 in cytosine [3]. Nitrogen mustards are characterized by high reactivity combined with the lack of sequence-specific binding of DNA. They rapidly lose their activity by non-specific interaction with a number of nucleophilic groups on cellular biomolecules other than DNA, which results in side effect, mutagenicity, teratogenicity, carcinogenicity and to promoting secondary malignancies [4–8]. However, the

* Corresponding author.
E-mail address: krzysztof.laczkowski@cm.umk.pl (K.Z. Łączkowski).

http://dx.doi.org/10.1016/j.molstruc.2016.04.058
0022-2860/

search for new substances that selectively inhibit the growth of cancer cells without damaging healthy cells is a very difficult problem.

In attempts to improve the selectivity and therapeutic efficacy researchers create hybrid molecules using nitrogen mustard derivatives and DNA binding pharmacophores, such as polyamides, acridines and 9-anilinoquinolines [9–11]. One of the most important results of this method is the development of Tallimustine-drug having an enhanced sequence-selectivity [12]. In our earlier study it has been observed that combining of thiazol-2-yl-hydrazine pharmacophore with the active anticancer nitrogen mustard moiety resulted in compounds with high antiproliferative activity against different human cancer cells. Additionally these hybrids were characterized by a low cytotoxicity against normal mouse fibroblast BALB/3T3 [13].

These results encouraged us to continue our investigation on the synthesis and molecular interaction of biologically active 2,4-disubstituted thiazoles [14–17]. Our research began with the design and synthesis of ten novel thiazole-based nitrogen mustards containing benzenesulfonamide pharmacophore, and evaluation of their antiproliferative activity against human cancer cells lines (biphenotypic B myelomonocytic leukemia MV4-11, human lung carcinoma A549, human breast carcinoma MCF-7, human colon carcinoma HCT116) and normal mouse fibroblast (BALB/3T3) using the 3-(4,5-dimethylthiazol-2-yl)-2,5-diphenyltetrazoliun bromide (MTT) or sulforhodamine B (SRB) assays. Moreover, spectroscopic characterization and cellular localization for selected compound were performed. Additionally, continuing our research on the interaction between the novel mustard drugs and nucleobases, we perform quantum chemical calculation of interaction and binding energies in complexes of the most active drugs with guanine. Finally, computer simulations were performed with DNA-binding site of hTopoI and hTopoII.

2. Results and discussion

2.1. Chemistry

Synthesis of target thiazole-based nitrogen mustards containing benzenesulfonamide moiety consists of two steps. In the first step appropriate benzenesulfonamide chloroacetophenones **2a-j** were prepared by sulfamidation reaction of 1-(4-aminophenyl)-2-chloroethanone (**1**) with different substituted chlorobenzenesulfonamides in pyridine at room temperature, with 22–55% yield and high purity (Scheme 1). In the next step, a series of thiazole-based nitrogen mustard derivatives **5a-j** were synthesized by Hantzsch condensation reaction between different substituted benzenesulfonamide chloroacetophenones **2a-j** and the 2-(4-(bis(2-chloroethyl)amino)benzylidene)hydrazinecarbothioamide (**4**) [13,18] in refluxing absolute ethyl alcohol, with high yield (48–97%) in order to explore the SARs of these derivatives and to obtain potential leading compounds. All of the synthesized derivatives were purified and their structures were characterized by spectroscopic methods ^{1}H NMR (700 and 400 MHz) and ^{13}C NMR (100 MHz), FAB(+)-MS and elemental analyses. ^{1}H NMR spectrum of thiazoles showed singlet at δ (7.11–7.88) due to thiazole-5H proton, which confirms the conversion of substrates in to the expected products. The characteristic proton of CH=N group occurs in the spectra around 7.70–8.23 ppm. The mass spectra of all compounds are fully consistent with the assigned structures. The elemental analyses values are in good agreement with the calculated values confirming the formation of analytically pure products. All reactions were repeated at least two times and are fully reproducible.

2.2. Biological evaluation

Results of the *in vitro* studies on antiproliferative activity of compounds **5a-j** against four human cancer cell lines (MV4-11, A549, MCF-7 and HCT116) and normal mouse fibroblast (BALB/3T3) using *cis*-platin as positive control are summarized in Table 1. In our study, compounds with IC_{50} below 4 μg/ml are consider as potential drugs [19]. We started our research from testing all compounds against biphenotypic B myelomonocytic leukemia MV4-11 cells. Selected five highly active compounds **5b**, **5c**, **5e**, **5f** and **5i** with IC_{50} values between 2.17 and 4.26 μg/ml were next tested against cancer cell lines A549, MCF-7, HCT116 and normal cell line BALB/3T3.

According to our results, compound **5e** has very strong activity against human lung carcinoma A549, human breast carcinoma MCF-7, and human colon carcinoma HCT116, with IC_{50} values from 3.03 to 4.99 μg/ml. The cytotoxic activity of compound **5e** against normal mouse fibroblast BALB/3T3 cells is 5–8 times lower than against cancer cell lines.

Our data indicated also that compound **5f** has very strong activity against human lung carcinoma A549 and human breast carcinoma MCF-7, with IC_{50} 4.58 μg/ml and 4.18 μg/ml, respectively. This compound did not have cytotoxic activity against normal mouse fibroblast BALB/3T3 cells.

Also compound **5i** has very strong activity against MCF-7 and HCT116 cell lines, with IC_{50} 3.42 μg/ml and 3.02 μg/ml, respectively.

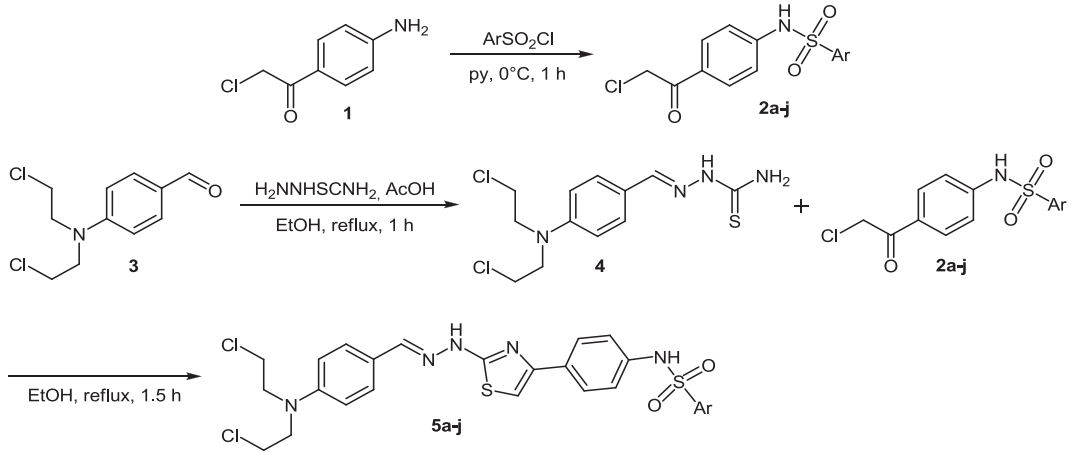

Scheme 1. Thiazole-based nitrogen mustard **5a-j**.

Table 1
Antiproliferative activity of thiazole-based nitrogen mustards **5a-j** against cancer cell lines MV4-11, A549, MCF-7, HCT116 and against normal mice fibroblast BALB/3T3.

Nitrogen mustards	Ar	IC_{50} [μg/ml]					logP
		MV4-11	A549	MCF-7	HCT116	Balb/3T3	
5a		14.05 ± 5.73	–	–	–	–	5.83
5b	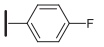	3.63 ± 1.07	6.13 ± 0.81	9.23 ± 3.42	42.26 ± 9.52	68.85 ± 28.3	6.15
5c	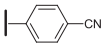	3.95 ± 1.88	10.29 ± 6.35	8.3 ± 3.06	28.34 ± 5.73	>100	5.74
5d	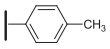	32.68 ± 6.37	–	–	–	–	6.29
5e	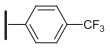	3.29 ± 0.77	4.99 ± 1.53	3.03 ± 0.58	4.13 ± 1.73	24.7 ± 7.4	6.80
5f	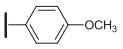	4.26 ± 1.67	4.58 ± 2.18	4.16 ± 1.67	43.38 ± 4.16	>100	6.35
5g	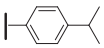	54.92 ± 13.87	–	–	–	–	7.17
5h	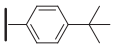	44.63 ± 16.9	–	–	–	–	7.52
5i	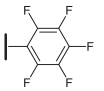	2.17 ± 1.02	20.52 ± 4.27	3.42 ± 0.27	3.02 ± 0.86	3.2 ± 0.6	6.53
5j	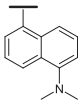	>100	–	–	–	–	7.52
cis-platin		0.31 ± 0.07	2.03 ± 0.31	2.46 ± 0.63	3.01 ± 1.11	1.4 ± 0.55	–

Lipophilic parameter, logP, was calculated for each molecule by using ACDlogP program, http://www.acdlabs.com.

This activity is similar to the activity of the most commonly used anticancer agent *cis*-platin. Cytotoxic activity of **5i** against normal mouse fibroblast BALB/3T3 is similar (IC_{50} 3.2 μg/ml), but still 2 times smaller than cytotoxicity of *cis*-platin (IC_{50} 1.4 μg/ml).

Compounds **5b** and **5c** show good activity against human lung carcinoma A549 and human breast carcinoma MCF-7, with IC_{50} 6.13–10.23 μg/ml. This compounds also did not have cytotoxic activity against normal mouse fibroblast BALB/3T3. Compounds **5a**, **5d**, **5g, 5h** and **5j** have no or very low antiproliferative activity against MV4-11 cell line.

Based on IC_{50} values we tried to establish a correlation between the activity of the derivatives and their chemical structure and in particular the nature of the functional groups. As can be easily noticed, the highest activity is observed in the case of compounds possessing electron-withdrawing groups (**5b**, **5c**, **5e** and **5i**). Within the tested series, compound **5f** containing electron-donating methoxy group also shows high activity. It is worth noticing that the compounds containing electron-donating methyl (**5d**), *iso*-propyl (**5g**) and *tert*-butyl (**5h**) groups exhibit only very low activity. As a result of our research, we have identified new substituents ($NHSO_2CF_3$ (**5e**) and $NHSO_2C_6F_5$ (**5i**)) which significantly enhance antiproliferative activity in almost all tested cancer cell lines MV4-11, A549, MCF-7 and HCT116.

2.3. Spectroscopic properties

Permeability across biological membranes is a key factor in the absorption and distribution of drugs [20]. Due to the presence of the fluorescent dansyl group in compound **5j** we decided to determine the possible place of accumulation of this compound in cancer cell using spectroscopic methods and take on trying to explain the lack of activity of some nitrogen mustard derivatives. For this purpose, as the first step we determined spectroscopic properties of the compound **5j**.

Absorption spectra of synthesized compound **5j** consists of three bands in the range of 250–420 nm with local maxima at 265, 308 and 367 nm (Fig. 1a). Molar absorption coefficients for each particular band are relatively high (over 10^3) what allow to classify them as intense and implicates the $\pi \rightarrow \pi^*$ type of transitions (Table 2) The maximum of fluorescence spectra is observed at 530 nm (Fig. 1b), what implies the emission in the range of visible light and a quite large Stokes shift (8380 cm^{-1}, 163 nm). Such a big difference between absorption and emission maxima is highly desired since it is critical for the sensitivity of fluorescent methods. In many cases this type of red-shift is connected with solvatochromism and big change in dipole moments between ground and excited states. However, in this case our studies did not reveal any relationships between solvent polarity and emission wavelength. For quantitative description of fluorescence phenomenon the quantum yield has been calculated according to standard dye and counts 0.05. This is relatively small value but still may be usable in cellular imaging *in vitro*.

To gain a deeper understanding of spectroscopic properties of newly synthesized compound **5j**, theoretical calculations have been carried out. For this task we applied Time-Dependent Density Functional Theory with the B3LYP functional, using the 6-31 + G (d,p) basis set (TD-DFT/B3LYP/6-31 + G (d,p)) with PCM model. The results, that include main electronic transitions with relatively high oscillator strength in every band, are presented in Table 3. The transitions which are responsible for the corresponding experimental absorption maxima are highlighted. The rest of calculated electronic transitions were omitted since they have small oscillator strength and constitute only a background for absorption bands. As we can see, the calculated value of wavelengths at spectra maxima

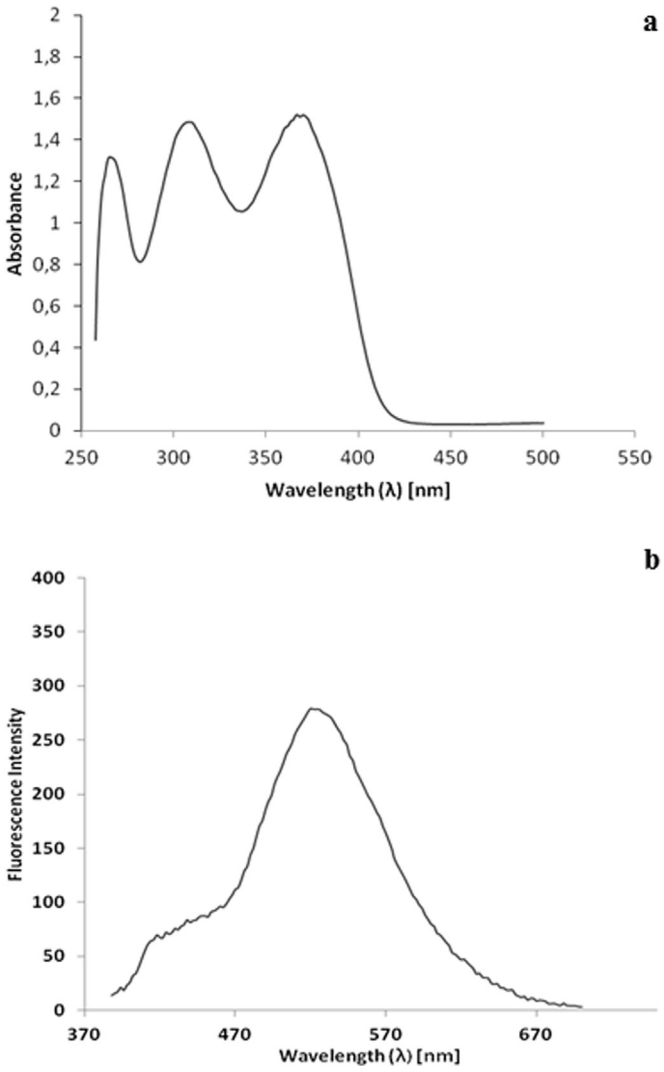

Fig. 1. Absorption (concentration 5×10^{-5} M) and fluorescence (concentration 6.25×10^{-7} M) spectra of **5j** dye solution in DMSO.

Table 2
Spectroscopic properties of **5j** solution in DMSO.

Absorption data		Emission data		
λ_{abs}/nm	$\varepsilon \cdot 10^3$/M^{-1} cm^{-1}	λ_{max}/nm	Stokes shift/nm	ϕ
367	30.4	530	163	0.05
308	29.5			
266	26.7			

are in excellent correspondence with experimental data. The biggest difference relates to maximum of the first absorption band and amounts to 12 nm, what represents only 3% error. The spectra prediction based on TD-DFT calculations also confirms correctness of these results (Fig. 2).

Visualization of molecular orbitals involved in main electronic transitions lets for better analysis of changes in molecule taking place during excitation process. According to our calculations, we can assume that the first absorption band is assigned to four transitions $S_0 \rightarrow S_1$, $S_0 \rightarrow S_2$, $S_0 \rightarrow S_3$ and $S_0 \rightarrow S_4$. The $S_0 \rightarrow S_3$ transition with the largest oscillatory strength is responsible for maximum of this band, what arises from a good overlap of involved orbitals – HOMO and $LUMO_{+1}$ whose electron distribution is located on the first phenyl and thiazole rings. The similar situation occurs for $S_0 \rightarrow S_2$ transition, which employs $HOMO_{-1}$ and LUMO orbitals located on the naphthalene ring. On the other hand, comparison of the electron distribution of HOMO and LUMO orbitals indicates the strong charge-transfer (CT) character of $S_0 \rightarrow S_1$ transition what explains the low oscillator strength. In the case of second band, the most important transitions are $S_0 \rightarrow S_6$, $S_0 \rightarrow S_9$ and $S_0 \rightarrow S_7$ which is assigned to next experimental absorption maximum. All of them employs LUMOs orbital with higher energy – $LUMO_{+2}$ which is localized on the central part of molecule, partially on the first and the second phenyl ring and $LUMO_{+5}$ together with $LUMO_{+4}$ whose electron distribution is concentrated mainly on the first phenyl ring and second phenyl ring respectively. The $S_0 \rightarrow S_{19}$ transition responsible for third absorption maximum is due to two molecular orbital contributions -$HOMO_{-6} \rightarrow$ LUMO and $HOMO_{-4} \rightarrow LUMO_{+3}$ which embrace only naphthalene part of the molecule. While electron distribution of orbitals involved in $S_0 \rightarrow S_{18}$ transition is spread on almost whole molecule, excluding the naphthalene ring. Shapes of all presented orbitals implicate the $\pi \rightarrow \pi^*$type of transitions in every case. Visualization of molecular orbitals involved in main electronic transition, obtained at the TD-DFT B3LYP/6-31 + G(d,p) theory level are given in the Supporting Information (S1).

The fluorescence emission energy for spin-allowed singlet-singlet ($S_n \rightarrow S_0$) transition was also calculated for dye solution in DMSO. Computed data including transition energy, oscillator strength, and orbitals involved in emission process, together with comparison of experimental data are given in Supporting Information. The agreement of calculated and experimental data, however less impressive is still in on good level for this type of calculation [21]. Noticeably HOMO and LUMO orbitals calculated for optimized geometry in ground and first excited state have different energy level and electron distribution, what reflects in emission process.

Using theoretical data, the attempt of explanation of large Stokes shift and low quantum yield was undertaken. Analysis of optimized geometry of S_0 and S_1 state delivered important information about changes in molecular framework after excitation. The main alterations occurs in coordinates of a central part of the molecule and are seen as a new plane created with thiazole and second phenyl rings, see the Supporting Information (S2). As a result of this comparison, we are able to connect large Stokes shift with the geometry relaxation of molecule in excited state. Namely, the optimized geometry of ground and first singlet excited state differs significantly, what causes bigger difference between excitation and emission energy and larger Stokes shift [22,23]. Additionally, non-radiative process like internal conversion (IC) occurs resulting in loss of energy. According to Kasha's rule the emission (fluorescence or phosphorescence) occurs only from the lowest lying electronically excited singlet state S_1 [23]. Thus in our case, since the main transition is $S_0 \rightarrow S_3$ (HOMO $\rightarrow$ $LUMO_{+1}$) the molecule quickly relaxes to the lowest vibrational level (S_1 state, LUMO). From the change of electron distribution of LUMO and HOMO orbitals calculated for ground and excited state, conformation transformation is easily noticeable (see Supporting Information S3 and S4.

2.4. Cellular staining

The good spectroscopic properties of compound **5j** prompted us to perform cellular staining and co-localization experiments to gain more information on possible mechanism of action of the nitrogen mustard derivatives that have been tested.

The toxicity level appeared to be relatively low with 15 mM for HCT-116 as still safe concentration. This allows for convenient

Table 3
Electronic transition data obtained by TD-DFT/B3LYP/6-31 + G(d,p) using a PCM model (solvent – DMSO) for **5j** at the DFT optimized geometry of ground state.

	Electronic transition	Λ (nm)	F (nm)	Molecular orbital	Percentage contribution (%)	Experimental λ (nm)
Band 1	$S_0 \rightarrow S_1$	403.48	0.0252	HOMO → LUMO	97	367
	$S_0 \rightarrow S_2$	390.85	0.2562	$HOMO_{-1}$ → LUMO	94	
	$S_0 \rightarrow S_3$	379.50	1.1339	HOMO → $LUMO_{+1}$	94	
	$S_0 \rightarrow S_4$	346.80	0.2568			
Band 2	$S_0 \rightarrow S_6$	313.64	0.0414	$HOMO_{-1}$ → $LUMO_{+2}$	83	308
	$S_0 \rightarrow S_7$	306.90	0.1467			
	$S_0 \rightarrow S_9$	300.57	0.1373	HOMO → $LUMO_{+5}$	68	
				HOMO → $LUMO_{+4}$	17	
Band 3	$S_0 \rightarrow S_{18}$	267.17	0.1132	$HOMO_{-3}$ → $LUMO_{+1}$	63	266
				$HOMO_{-2}$ → $LUMO_{+4}$	10	
	$S_0 \rightarrow S_{19}$	265.27	0.1910	$HOMO_{-6}$ → LUMO	54	
				$HOMO_{-4}$ → $LUMO_{+3}$	19	

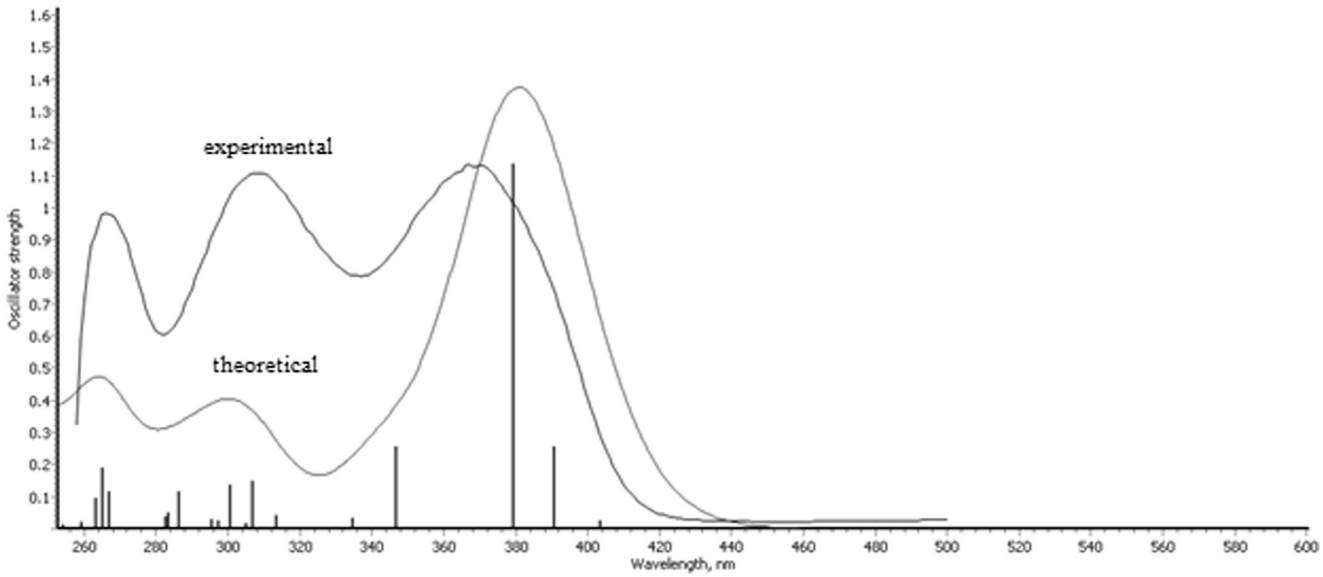

Fig. 2. Absorption **5j** dye spectra: experimental, measured in DMSO; theoretical, predicted basing on TD-DFT calculations.

visualization of the compound in the living cell without serious damage of its functions [24]. The tested compound **5j** effectively penetrated the membrane after 2 h incubation time. Its spectroscopic parameters allow to excitation with standard DAPI filter while the emission is, due to large Stockes shift, pushed to greenish region. Micrographs are presented in Supporting Information (S5). Intense signal from the cells visible in the micrographs, despite relatively low quantum yield of **5j** support its effective penetration through the membrane.

Apparently, this compound tends to accumulate primarily in cellular membrane and some extent in lysosomes. This undoubtedly is the result of the structure of this compound. Accumulation in cellular membrane and in lysosomes probably explains the complete lack of activity of compound **5j**, and also a small activity of compounds **5g** and **5h**. Relatively high lipophilicity, logP 7.17–7.52, and basic character due to nitrogen atoms are main factors affecting its intracellular behavior. Such compounds generally may exhibit lysosomotropism.

It has been shown that large lipophilicity of compounds promotes the accumulation of the drug in lysosomes [25]. We believe that this hinders their penetration into the cell nucleus (S5c) so that there is no alkylation of DNA located there. On the other hand we have found at least partial accumulation in mitochondria (S5b) and endoplasmic reticulum (S5a). These results confirm the possible DNA interaction in mitochondria. There are also reports on induction of endoplasmic reticulum stress by sulfur mustard derivatives [26]. It is tempting to hypothesize about similar effect in the tested compounds.

2.5. Interaction and binding energies in drug-guanine complexes

Nitrogen mustards are known to react with two guanine molecules, forming a bridge between two DNA strings, and mechanism of this reaction can be found in Ref. [27]. Our earlier study [13] focused of the interaction between thiazole moiety present in the recently developed nitrogen mustard and the four DNA bases, since the formation of such a drug-DNA base complex, with thiazole being an additional center helping in the formation of the bridge between the two DNA strings, can be important both, before and after reaction of chlorine atoms of nitrogen mustard with guanine. Our study revealed that out of the four DNA bases, the strongest hydrogen bonded complexes were formed with guanine, both in the case of model thiazoles and the real drug. As a continuation of that investigation, we presently carried out quantum chemical study of geometrical parameters, as well as interaction and binding energies, in the complexes formed by the new potential drugs and guanine.

Optimization of geometrical parameters of investigated complexes was carried out using Density Functional Theory with the B3LYP functional and the 6-311G** basis set, and was followed by

the evaluation of vibrational frequencies within the same approximation. To maximize the interaction between investigated drugs and guanine, in the starting geometries – one per complex – the two molecules were forming three hydrogen bonds. The optimized DFT/B3LYP/6-311G** structures together with the corresponding Cartesian coordinates geometries are reported in the Supporting Information. In Table 4 the hydrogen bond intermolecular distances (denoted as *r*, in Å) and angles (denoted as ∠, in deg) are reported.

Interaction energy of investigated complexes, $\Delta E(AB)$, is calculated as the difference between the energy of the complex (*AB*) and the energies of the monomers (*A* and *B*):

$$\Delta E(AB) = E^{AB}_{AB}(AB) - E^{AB}_{AB}(A) - E^{AB}_{AB}(B),$$

where $E^{B}_{G}(S)$ denotes energy of system *S* evaluated at the *G* optimized geometry using basis set *B*. Additionally, binding energies E_{bind} (*AB*) are calculated:

$$E_{bind}(AB) = \left[E^{AB}_{AB}(AB) - E^{AB}_{AB}(A) - E^{AB}_{AB}(B)\right] + \left[E^{A}_{AB}(A) - E^{A}_{A}(A)\right] + \left[E^{B}_{AB}(B) - E^{B}_{B}(B)\right],$$

to evaluate the size of geometry relaxation effects. Based on conclusions of our earlier work, evaluation of interaction and binding energies is carried out within the DFT/M06-2X/6-311++G** approximation. Results are reported in Table 4.

Analysis of binding energies reported in Table 4 reveals that the guanine complex with **5f** is the strongest (binding energy of −24.9 kcal/mol), followed by that with **5b** (−24.7 kcal/mol), **5e** (−24.3 kcal/mol), and **5c** (−24.2 kcal/mol). Much weaker interaction is observed for the complex **5i-G** (binding energy of only −19.0 kcal/mol). The observed differences in binding energies are reflected in the hydrogen bonding distances and angles. Interaction energies for the first four complexes reported in Table 4 are approximately 5 kcal/mol lower than the corresponding binding energies, and their values are practically identical for the complexes **5b-G** and **5f-G** (−29.5 kcal/mol), and for complexes **5c-G** and **5e-G** (−29.2 kcal/mol). This difference is close to the one reported in our previous study for the complex of the (*E*)-*N*-(4-(2-(2-(4-(bis(2-chloroethyl)amino)benzylidene)hydrazinyl)thiazol-4-yl) phenyl)methanesulfonamide with guanine, where the M06-2X/6-311++G** interaction energy was about 4 kcal/mol lower than the binding energy. In the case of the complex **5i-G** the interaction energy (−26.4 kcal/mol) is approximately 7 kcal/mol lower than the binding energy, indicating larger deformation of monomers' structure during formation of the **5i-G** complex than in the case of other complexes investigated here and previously. The first four complexes reported in Table 4 have larger values of interaction and binding energies than the (*E*)-*N*-(4-(2-(2-(4-(bis(2-chloroethyl) amino)benzylidene)hydrazinyl)thiazol-4-yl)phenyl)methanesulfonamide-guanine complex reported in our previous study [13].

2.6. Molecular modelling studies

Basic mechanism of anticancer activity of nitrogen mustard derivatives is connected with the process of DNA alkylation [3,27]. The resultant DNA adducts become apoptosis promotors and cause disturbing in the genetic material replication process. Nitrogen mustard derivatives, depending on their chemical structure, may have anticancer effect also due to activation or inactivation of other processes inside human cells. Inhibition of the topoisomerases is one of the effective mechanisms inhibiting the growth of cancer cells [28]. These enzymes take part in DNA metabolism in the broad sense, thus allowing the processes of replication, transcription, recombination and condensation of chromosomes. In order to check whether the biological activity of the synthesized compounds may also be connected with their interactions with human type I and II topoisomerases (hTopoI, hTopoII) computer simulations were performed. In our theoretical calculations the crystallographic models of DNA-binding domains of hTopoI (PDB id: 1SEU) and hTopoII (PDB id: 3QX3) were used. The total docking scores reflecting affinity of the analysed compounds (i.e., **5b**, **5c**, **5e**, **5f**, **5i**) towards hTopoI fell within the range between − 17.8 and − 24.2 kc al/mol vs. − 36.7 kc al/mol for the native ligand (Table 5). The lack of linear dependence between the affinity and activity of the analysed derivatives may be due to the specific nature of respective cancer cells lines, intensified activity of topoisomerases inside these cells and the effectiveness of DNA repair mechanisms. Moreover, the final pharmacological effect also depends on the difference in permeability through biological membranes of cancer cells.

Much better correlation between *in silico* and *in vitro* test results was obtained for hTopoII (PDB id: 3QX3). Compound **5i**, showing the highest affinity towards DNA-dependent subunit of this enzyme (−5.7 kcal/mol), was also the strongest inhibitor of colorectal cancer (HCT116) and leukaemia (MV4-11) cells growth, and second, as regards the effect against breast cancer cells (MCF-7). As shown in Fig. 3, the ligand–enzyme complex is stabilized by three hydrogen bonds with residues Asp479, Gln778, Ala779, one hydrogen bond with water molecule Hoh1461, and hydrophobic interaction of pentafluorophenyl moiety with Gln778. Compound **5f** showed docking score −4.2 kcal/mol and ranked second. It was mediating hydrogen bond interactions with the residues Gln778, Ala779, Glu447, Ala779 and water molecule Hoh1461. The methoxyphenyl ring of **5f** formed favorable hydrophobic contacts with Ala779 and Gln778. Although remaining compounds **5b**, **5c** and **5e** exhibited low docking scores (within the range

Table 5
Docking scores for active nitrogen mustards.

Enzyme	Docking scores (kcal/mol)					
	5b	5c	5e	5f	5i	Etoposide
hTopoI	−24.2	−23.9	−21.1	−20.9	−17.8	−36.7
hTopoII	−3.1	−3.2	−2.3	−4.2	−5.7	−10.1

Table 4
Selected DFT/B3LYP/6-311G** geometrical parameters characterizing hydrogen bonds present in the investigated complexes, and predicted DFT/M06-2X/6-311++G** interaction and binding energies.

Complex	r(N–H···N) [Å]	∠(NHN) [°]	r(N–H···O^1) [Å]	∠(NHO^1) [°]	r(N–H···O^2) [Å]	∠(NHO^2) [°]	ΔE [kcal/mol]	E_{bind} [kcal/mol]
5b-G	3.018	172.8	2.824	174.9	3.162	149.5	−29.5	−24.7
5c-G	3.008	172.1	2.831	174.6	3.165	149.8	−29.2	−24.2
5e-G	3.013	172.4	2.827	174.8	3.166	149.6	−29.2	−24.3
5f-G	3.039	173.5	2.810	175.2	3.188	147.5	−29.5	−24.9
5i-G	3.114	173.6	2.781	174.9	3.414	135.6	−26.4	−19.0

Symbol O^1 denotes oxygen atom in guanine molecule, and O^2 – oxygen atom of the SO_2 group forming the hydrogen bond.

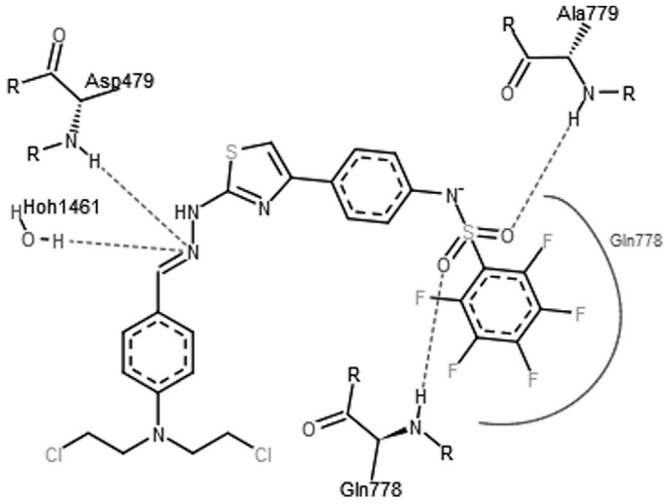

Fig. 3. Interactions between **5i** and the residues of the DNA-binding site of hTopoII.

between −2.3 and −3.2 kcal/mol vs. −10.1 kcal/mol for native ligand, Table 5) they were still stabilized by at least two hydrogen bonds with the residues Gln778, Ala779, Ser480, Leu502 and in the case of **5c** with water molecule Hoh1461. Moreover, the phenyl moiety of **5b**, **5c** and **5e** at sulfonamide group formed favorable hydrophobic contacts with Gln778, Met782, Ala779. In conclusion, the present results indicating the possibility of human topoisomerases inhibition as one of the mechanisms of anticancer effect of the synthesized derivatives (Fig. 4).

3. Conclusion

In summary, we have developed an efficient method for the synthesis of thiazole-based nitrogen mustard. As a result of our research, we have identified new substituent ($NHSO_2CF_3$) which significantly enhanced antiproliferative activity in all tested cancer cell lines MV4-11, A549, MCF-7 and HCT116. Among the derivatives, **5b**, **5c**, **5e**, **5f** and **5i** were found to exhibit high activity against human leukaemia MV4-11 cells, with IC_{50} values of 2.17–4.26 μg/ml. The cytotoxic activity of compounds **5e** against normal mouse fibroblast BALB/3T3 cells is 5–8 times lower than against cancer cell lines. Spectroscopic studies show that the model compound **5j** tends to accumulate in cellular membrane and to some extent in lysosomes, which probably explains the complete lack of activity of some tested compounds, while partial accumulation in mitochondria and endoplasmic reticulum explains their plausible mechanism of activity. The molecular modelling studies indicating the possibility of human topoisomerases inhibition as one of the mechanisms of anticancer effect of the synthesized derivatives.

4. Experimental

4.1. Materials and methods

All experiments were carried out under air atmosphere unless stated otherwise. Reagents were generally the best quality commercial-grade products and were used without further purification. ^{1}H NMR (700 and 400 MHz) and ^{13}C NMR (100 MHz) spectra were recorded on a Bruker Avance III multinuclear instrument. FAB(+)-MS was performed by the Laboratory for Analysis of Organic Compounds and Polymers of the Centre for Molecular and Macromolecular Studies of the Polish Academy of Science in Łódź. MS spectra were recorded on a Finnigan MAT 95 spectrometer.

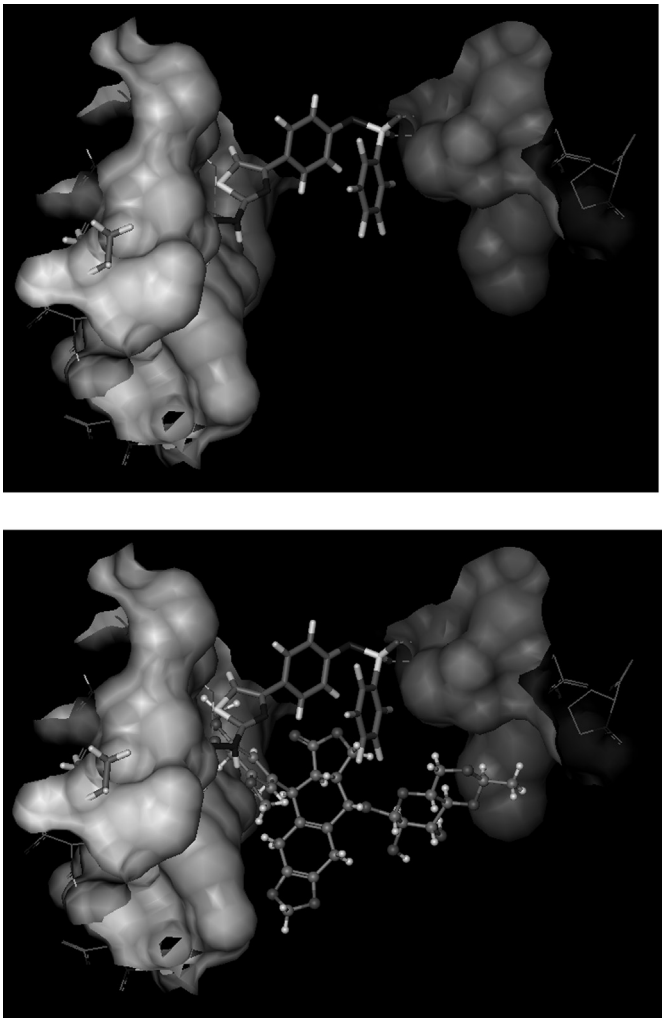

Fig. 4. Docking results with DNA-binding domain of hTopoII. Binding mode of **5i** (*up*); binding mode of **5i** and etoposide (native ligand) (*down*).

Elemental analysis was performed on ELEMENTAR Vario MACRO CHN. Melting points were determined in open glass capillaries and are uncorrected. Analytical TLC was performed using Macherey-Nagel Polygram Sil G/UV_{254} 0.2 mm plates. 4-(Bis(2-chloroethyl) amino)benzaldehyde, chlorobenzenesulfonamides, acetic acid, thiosemicarbazide, pyridine were commercial materials (Aldrich).

4.1.1. *N-(4-(2-Chloroacetyl)phenyl)benzenesulfonamide (2a). Typical procedure*

Benzenesulfonyl chloride (0.52 g, 2.95 mmol) was added to a stirred solution of 1-(4-aminophenyl)-2-chloroethanone (**1**) (0.50 g, 2.95 mmol) in dry pyridine (6 ml) at 0 °C. The reaction mixture was stirred under room temperature for 2.5 h under nitrogen atmosphere. After that, 10% hydrochloric acid solution (40 ml) was added and the product was filtered off and subsequently washed with water. The separated precipitate was purified on silica gel column chromatography (230–400 mesh) using (dichloromethane/methanol, 90:10, $R_f = 0.83$) to afford the desired product: 0.50 g, 55%; mp 172–175 °C. ^{1}H NMR (DMSO-d_6, 400 MHz), δ (ppm): 5.06 (s, 2H, CH_2); 7.23 (d, 2H, 2CH, J = 9.0 Hz); 7.56–7.67 (m, 3H, 3CH); 7.83–7.88 (m, 4H, 4CH); 10.98 (s, 1H, NH). ^{13}C NMR (DMSO-d_6, 100 MHz), δ (ppm): 47.84; 118.29 (2C); 127.17 (2C); 129.71; 129.99 (2C); 130.56 (2C); 133.83; 139.66; 143.30; 190.54. *Anal.* Calcd. for $C_{14}H_{12}ClNO_3S$: C, 54.28; H, 3.90; N, 4.52.

Found: C, 54.31; H, 3.91; N, 4.54.

4.1.2. N-(4-(2-Chloroacetyl)phenyl)-4-fluorobenzenesulfonamide (2b)

4-Fluorobenzene-1-sulfonyl chloride was reacted with **1**. Yield: 0.40 g, 41%, (dichloromethane/methanol, 90:10, R_f = 0.78); mp 156–158 °C. ^{1}H NMR (DMSO-d_6, 400 MHz), δ (ppm): 5.07 (s, 2H, CH_2); 7.24 (d, 2H, 2CH, J = 9.0 Hz); 7.40–7.46 (m, 2H, 2CH); 7.87 (d, 2H, 2CH, J = 9.0 Hz); 7.90–7.94 (m, 2H, 2CH); 11.00 (s, 1H, NH). ^{13}C NMR (DMSO-d_6, 100 MHz), δ (ppm): 47.84; 117.20 (2C); 118.49 (2C); 129.85; 130.33 (2C); 130.56 (2C); 136.03; 143.15; 166.24; 190.57. *Anal*. Calcd. for $C_{14}H_{11}ClFNO_3S$: C, 51.30; H, 3.38; N, 4.27. Found: C, 51.31; H, 3.37; N, 4.30.

4.1.3. N-(4-(2-Chloroacetyl)phenyl)-4-cyanobenzenesulfonamide (2c)

4-Cyanobenzene-1-sulfonyl chloride was reacted with **1**. Yield: 0.30 g, 30%, (dichloromethane/methanol, 90:10, R_f = 0.76); mp 196–198 °C. ^{1}H NMR(DMSO-d_6, 400 MHz), δ (ppm): ^{1}H NMR (DMSO-d_6, 400 MHz), δ (ppm): 5.07 (s, 2H, CH_2); 7.24 (d, 2H, 2CH, J = 9.0 Hz); 7.88 (d, 2H, 2CH, J = 9.0 Hz); 8.00 (d, 2H, 2CH, J = 9.0 Hz); 8.07 (d, 2H, 2CH, J = 9.0 Hz); 11.23 (s, 1H, NH). ^{13}C NMR (DMSO-d_6, 100 MHz), δ (ppm): 47.87; 116.25; 117.93; 118.82 (2C); 127.93 (2C); 130.22; 130.63 (2C); 134.19 (2C); 142.62; 143.64; 190.60. *Anal*. Calcd. for $C_{15}H_{11}ClN_2O_3S$: C, 53.82; H, 3.31; N, 8.37. Found: C, 53.82; H, 3.30; N, 8.40.

4.1.4. N-(4-(2-Chloroacetyl)phenyl)-4-methylbenzenesulfonamide (2d)

4-Methylbenzene-1-sulfonyl chloride was reacted with **1**. Yield: 0.26 g, 27%, (dichloromethane/methanol, 90:10, R_f = 0.77); mp 182–184 °C. ^{1}H NMR (DMSO-d_6, 400 MHz), δ (ppm): 2.33 (s, 3H, CH_3); 5.05 (s, 2H, CH_2); 7.22 (d, 2H, 2CH, J = 9.0 Hz); 7.37 (d, 2H, 2CH, J = 9.0 Hz); 7.74 (d, 2H, 2CH, J = 9.0 Hz); 8.85 (d, 2H, 2CH, J = 9.0 Hz); 10.90 (s, 1H, NH). ^{13}C NMR (DMSO-d_6, 100 MHz), δ (ppm): 21.43; 47.81; 118.17 (2C); 127.23 (2C); 129.59; 130.39 (2C); 130.54 (2C); 136.81; 143.43; 144.29; 190.53. *Anal*. Calcd. for $C_{15}H_{14}ClNO_3S$: C, 55.64; H, 4.36; N, 4.33. Found: C, 55.62; H, 4.34; N, 4.36.

4.1.5. N-(4-(2-Chloroacetyl)phenyl)-4-(trifluoromethyl) benzenesulfonamide (2e)

4-(Trifluoromethyl)benzene-1-sulfonyl chloride was reacted with **1**. Yield: 0.35 g, 32%, (dichloromethane/methanol, 90:10, R_f = 0.86); mp 153–155 °C. ^{1}H NMR (DMSO-d_6, 400 MHz), δ (ppm): 5.07 (s, 2H, CH_2); 7.25 (d, 2H, 2CH, J = 9.0 Hz); 7.88 (d, 2H, 2CH, J = 9.0 Hz); 7.99 (d, 2H, 2CH, J = 9.0 Hz); 8.06 (d, 2H, 2CH, J = 9.0 Hz); 11.20 (s, 1H, NH). ^{13}C NMR (DMSO-d_6, 100 MHz), δ (ppm): 48.79; 119.78 (2C); 123.98; 125.48; 128.28 (q, J_{C-F} = 4.0 Hz); 129.19 (2C); 131.16; 131.63 (2C); 134.29 (q, J_{C-F} = 32.0 Hz); 143.74; 144.60; 191.58. *Anal*. Calcd. for $C_{15}H_{11}ClF_3NO_3S$: C, 47.69; H, 2.93; N, 3.71. Found: C, 47.70; H, 3.95; N, 3.73.

4.1.6. N-(4-(2-Chloroacetyl)phenyl)-4-methoxybenzenesulfonamide (2f)

4-Methoxybenzene-1-sulfonyl chloride was reacted with **1**. Yield: 0.38 g, 38%, (dichloromethane/methanol, 90:10, R_f = 0.84); mp 139–142 °C. ^{1}H NMR (DMSO-d_6, 400 MHz), δ (ppm): 3.80 (s, 3H, CH_3); 5.06 (s, 2H, CH_2); 7.09 (d, 2H, 2CH, J = 9.0 Hz); 7.22 (d, 2H, 2CH, J = 9.0 Hz); 7.78 (d, 2H, 2CH, J = 9.0 Hz); 7.85 (d, 2H, 2CH, J = 9.0 Hz); 10.84 (s, 1H, NH). ^{13}C NMR (DMSO-d_6, 100 MHz), δ (ppm): 47.82; 56.14; 115.08 (2C); 118.06 (2C); 129.48 (2C); 130.54 (2C); 131.18; 131.44; 143.54; 163.20; 190.52. *Anal*. Calcd. for $C_{15}H_{14}ClNO_4S$: C, 53.02; H, 4.15; N, 4.12. Found: C, 53.00; H, 4.14; N, 4.15.

4.1.7. N-(4-(2-Chloroacetyl)phenyl)-4-isopropylbenzenesulfonamide (2g)

4-Isopropylbenzene-1-sulfonyl chloride was reacted with **1**. Yield: 0.28 g, 27%, (dichloromethane/methanol, 90:10, R_f = 0.76); mp 149–150 °C. ^{1}H NMR (DMSO-d_6, 400 MHz), δ (ppm): 1.17 (d, 6H, $2CH_3$, J = 7.0 Hz); 2.94 (sept., 1H, CH, J = 7.0 Hz); 3.80 (s, 3H, CH_3); 5.06 (s, 2H, CH_2); 7.24 (d, 2H, 2CH, J = 9.0 Hz); 7.46 (d, 2H, 2CH, J = 9.0 Hz); 7.78 (d, 2H, 2CH, J = 9.0 Hz); 7.87 (d, 2H, 2CH, J = 9.0 Hz); 10.95 (s, 1H, NH). ^{13}C NMR (DMSO-d_6, 100 MHz), δ (ppm): 23.79 (2C); 33.80; 47.81; 118.00 (2C); 127.34 (2C); 127.92 (2C); 129.53; 130.59 (2C); 137.29; 143.46; 154.62; 190.51. *Anal*. Calcd. for $C_{17}H_{18}ClNO_3S$: C, 58.03; H, 5.16; N, 3.98. Found: C, 58.00; H, 5.15; N, 4.00.

4.1.8. 4-tert-Butyl-N-(4-(2-chloroacetyl)phenyl) benzenesulfonamide (2 h)

4-*tert*-Butylbenzene-1-sulfonyl chloride was reacted with **1**. Yield: 0.33 g, 30%, (dichloromethane/methanol, 90:10, R_f = 0.74); mp 152–153 °C. ^{1}H NMR (DMSO-d_6, 400 MHz), δ (ppm): 1.26 (s, 9H, $3CH_3$); 5.06 (s, 2H, CH_2); 7.25 (d, 2H, 2CH, J = 9.0 Hz); 7.61 (d, 2H, 2CH, J = 9.0 Hz); 7.79 (d, 2H, 2CH, J = 9.0 Hz); 7.87 (d, 2H, 2CH, J = 9.0 Hz); 10.97 (s, 1H, NH). ^{13}C NMR (DMSO-d_6, 100 MHz), δ (ppm): 31.14 (3C); 35.37; 47.79; 117.94 (2C); 126.85 (2C); 127.07 (2C); 129.51; 130.61 (2C); 137.05; 143.48; 156.82; 190.50. *Anal*. Calcd. for $C_{18}H_{20}ClNO_3S$: C, 59.09; H, 5.51; N, 3.83. Found: C, 59.11; H, 5.49; N, 3.84.

4.1.9. N-(4-(2-Chloroacetyl)phenyl)-2,3,4,5,6-pentafluorobenzenesulfonamide (2i)

2,3,4,5,6-Pentafluorobenzene-1-sulfonyl chloride was reacted with **1**. Yield: 0.26 g, 22%, (dichloromethane/methanol, 90:10, R_f = 0.84); mp 165–168 °C. ^{1}H NMR (DMSO-d_6, 400 MHz), δ (ppm): 5.10 (s, 2H, CH_2); 7.28 (d, 2H, 2CH, J = 9.0 Hz); 7.95 (d, 2H, 2CH, J = 9.0 Hz); 12.00 (s, 1H, NH). ^{13}C NMR (DMSO-d_6, 100 MHz), δ (ppm): 47.86; 113.06; 115.15 (m); 118.83 (2C); 130.73 (2C); 131.41; 136.86 (m); 139.39 (m); 141.73; 143.26 (m); 145.80 (m); 190.71. *Anal*. Calcd. for $C_{14}H_7ClF_5NO_3S$: C, 42.07; H, 1.77; N, 3.50. Found: C, 42.06; H, 1.74; N, 3.51.

4.1.10. N-(4-(2-Chloroacetyl)phenyl)-5-(dimethylamino) naphthalene-1-sulfonamide (2j)

5-(Dimethylamino)naphthalene-1-sulfonyl chloride was reacted with **1**. Yield: 0.61 g, 51%, (dichloromethane/methanol, 90:10, R_f = 0.76); mp 89–91 °C. ^{1}H NMR (DMSO-d_6, 400 MHz), δ (ppm): 2.81 (s, 6H, $2CH_3$); 5.00 (s, 2H, CH_2); 7.17 (d, 2H, 2CH, J = 9.0 Hz); 7.28 (d, 1H, CH, J = 8.0 Hz); 7.62–7.69 (m, 2H, 2CH); 7.79 (d, 2H, 2CH, J = 9.0 Hz); 8.32–8.38 (m, 2H, 2CH); 8.48 (d, 1H, CH, J = 8.0 Hz); 11.35 (s, 1H, NH). ^{13}C NMR (DMSO-d_6, 100 MHz), δ (ppm): 45.50 (2C); 47.72; 115.91; 117.31 (2C); 118.74; 124.07; 128.96; 129.20; 129.29; 129.47; 130.53 (2C); 130.67; 131.08; 134.63; 143.22; 152.03; 190.41. *Anal*. Calcd. for $C_{20}H_{19}ClN_2O_3S$: C, 59.62; H, 4.75; N, 6.95. Found: C, 59.60; H, 4.72; N, 6.94.

4.1.11. (E)-2-(4-(Bis(2-chloroethyl)amino)benzylidene) hydrazinecarbothioamide (4)

4-(Bis-(2-chloroethyl)amino)benzaldehyde (**3**) (2.00 g, 8.12 mmol) in ethyl alcohol (20 ml) was added to a stirred hot solution of thiosemicarbazide (0.74 g, 8.12 mmol) in water (24 ml) and then (1.6 ml) glacial acetic acid was added. The reaction mixture was stirred under reflux for 1 h, cooled to room temperature and separate yellow precipitate was collected by filtration. Yield: 2.38 g, 92%; mp 192–193 °C [13,18]. ^{1}H NMR (400 MHz, DMSO-d_6) δ (ppm): 3.77 (m, 8H, $4CH_2$); 6.77 (d, 2H, 2CH, J = 9.0 Hz); 7.60 (d, 2H, 2CH,

J = 9.0 Hz); 7.77 (bs, 1H, NH); 7.93 (bs, 1H, NH); 8.02 (bs, 1H, NH); 11.21 (s, 1H, CH). ^{13}C NMR (DMSO-d_6, 100 MHz) δ (ppm): 41.54 (2C); 52.33 (2C); 112.20 (2C); 123.05; 129.42 (2C); 143.36; 148.34; 177.68.

4.1.12. (E)-N-(4-(2-(2-(4-(Bis(2-chloroethyl)amino)benzylidene) hydrazinyl)thiazol-4-yl)phenyl)benzenesulfonamide (5a). Typical procedure

Thiosemicarbazone **4** (0.26 g, 0.81 mmol) was added to a stirred solution of *N*-(4-(2-chloroacetyl)phenyl)benzene-sulfonamide (**2a**) (0.25 g, 0.81 mmol) in absolute ethyl alcohol (15 ml). The reaction mixture was under reflux for 1.5 h, cooled to room temperature and separate precipitate was collected by filtration. The crude product was purified on silica gel column chromatography (230–400 mesh) using (dichloromethane/methanol, 90:10, R_f = 0.79) to afford the desired product: 0.24 g, 52%; mp 187–190 °C with decomp. ^{1}H NMR (DMSO-d_6, 700 MHz), δ (ppm): 3.69–3.80 (m, 8H, 4CH_2); 6.80 (d, 2H, 2CH, J = 9.0 Hz); 7.11–7.14 (m, 3H, 3CH); 7.49 (d, 2H, 2CH, J = 9.0 Hz); 7.51–7.56 (m, 2H, 2CH); 7.58–7.61 (m, 1H, CH); 7.68 (d, 2H, 2CH, J = 9.0 Hz); 7.75–7.79 (m, 2H, 2CH); 7.95 (s, 1H, CH); 10.43 (bs, 1H, NH); 12.00 (bs, 1H, NH). ^{13}C NMR (DMSO-d_6, 100 MHz), δ (ppm): 41.48 (2C); 52.35 (2C); 103.18; 112.35 (2C); 119.73; 120.42 (2C); 122.90; 127.10; 127.15 (2C); 128.77; 129.45; 129.75 (2C); 133.43; 137.90; 139.91; 144.65; 146.21; 147.52; 148.22; 168.77. FAB(+)-MS (m/z, %): 574.2 [(M^++1), 100], 331.2 (28), 247.1 (60), 245.1 (100), 230.1 (24), 195.1 (64), 190.0 (80), 188.0 (100), 167.0 (36), 133.0 (28). *Anal.* Calcd. for $C_{26}H_{25}Cl_2N_5O_2S_2$: C, 54.35; H, 4.39; N, 12.19. Found: C, 54.36; H, 4.42; N, 12.22.

4.1.13. (E)-N-(4-(2-(2-(4-(Bis(2-chloroethyl)amino)benzylidene) hydrazinyl)thiazol-4-yl)phenyl)-4-fluorobenzene-sulfonamide (5b)

N-(4-(2-Chloroacetyl)phenyl)-4-fluorobenzenesulfonamide (**2b**) was reacted with **4**. Yield: 0.21 g, 58%, (dichloromethane/methanol, 90:10, R_f = 0.70); mp 195–198 °C with decomp. ^{1}H NMR (DMSO-d_6, 700 MHz), δ (ppm): 3.69–3.80 (m, 8H, 4CH_2); 6.80 (d, 2H, 2CH, J = 9.0 Hz); 7.12 (d, 2H, 2CH, J = 9.0 Hz); 7.14 (s, 1H, CH); 7.37–7.41 (m, 2H, 2CH); 7.48 (d, 2H, 2CH, J = 9.0 Hz); 7.69 (d, 2H, 2CH, J = 9.0 Hz); 7.80–7.84 (m, 2H, 2CH); 7.93 (s, 1H, CH); 10.42 (bs, 1H, NH); 11.90 (bs, 1H, NH). ^{13}C NMR (DMSO-d_6, 100 MHz), δ (ppm): 41.49 (2C); 52.36 (2C); 103.21; 112.36 (2C); 116.96 (2C); 119.94; 120.74 (2C); 123.03; 127.06 (2C); 128.67 (2C); 130.23 (2C); 136.24; 137.56; 144.12; 148.15; 163.54; 166.04; 168.80. FAB(+)-MS (m/z, %): 592.1 [(M^++1), 100], 349.1 (24), 247.1 (44), 245.1 (76), 230.1 (20), 207.1 (32), 195.1 (44), 190.0 (52), 188.1 (64), 181,.1 (40), 167.0 (24), 131.0 (20). *Anal.* Calcd. for $C_{26}H_{24}Cl_2FN_5O_2S_2$: C, 52.70; H, 4.08; N, 11.82. Found: C, 52.68; H, 4.10; N, 11.84.

4.1.14. (E)-N-(4-(2-(2-(4-(Bis(2-chloroethyl)amino)benzylidene) hydrazinyl)thiazol-4-yl)phenyl)-4-cyanobenzene-sulfonamide (5c)

N-(4-(2-Chloroacetyl)phenyl)-4-cyanobenzenesulfonamide (**2c**) was reacted with **4**. Yield: 0.18 g, 56%, (dichloromethane/methanol, 90:10, R_f = 0.73); mp 160 °C with decomp. ^{1}H NMR (DMSO-d_6, 700 MHz), δ (ppm): 3.72–3.80 (m, 8H, 4CH_2); 6.79 (d, 2H, 2CH, J = 9.0 Hz); 7.10 (d, 2H, 2CH, J = 9.0 Hz); 7.15 (s, 1H, CH); 7.47 (d, 2H, 2CH, J = 9.0 Hz); 7.70 (d, 2H, 2CH, J = 9.0 Hz); 7.89 (s, 1H, CH); 7.90 (d, 2H, 2CH, J = 9.0 Hz); 8.04 (d, 2H, 2CH, J = 9.0 Hz); 10.59 (bs, 1H, NH); 11.85 (bs, 1H, NH). ^{13}C NMR (DMSO-d_6, 100 MHz), δ (ppm): 41.49 (2C); 52.36 (2C); 103.36; 112.36 (2C); 115.86; 118.00; 120.29; 121.11 (2C); 122.70; 123.09; 127.09; 127.89; 127.92 (2C); 128.60; 133.90; 133.96 (2C); 136.91; 143.72; 143.90; 148.07; 168.84. FAB(+)-MS (m/z, %): 599.2 [(M^++1), 56], 356.2 (28), 247.1 (32), 245.1 (52), 195.1 (60), 173.1 (100), 167.0 (50), 149.0 (60), 136.0 (64). *Anal.* Calcd. for $C_{27}H_{24}Cl_2N_6O_2S_2$: C, 54.09; H, 4.03; N, 14.02. Found: C, 54.07; H, 4.03; N, 14.05.

4.1.15. (E)-N-(4-(2-(2-(4-(Bis(2-chloroethyl)amino)benzylidene) hydrazinyl)thiazol-4-yl)phenyl)-4-methylbenzene-sulfonamide (5d)

N-(4-(2-Chloroacetyl)phenyl)-4-methylbenzenesulfonamide (**2d**) was reacted with **4**. Yield: 0.22 g, 61%, (dichloromethane/methanol, 90:10, R_f = 0.82); mp 168-179 °C with decomp. ^{1}H NMR (DMSO-d_6, 700 MHz), δ (ppm): 2.32 (s, 3H, CH_3); 3.68–3.80 (m, 8H, 4CH_2); 6.79 (d, 2H, 2CH, J = 9.0 Hz); 7.05 (d, 2H, 2CH, J = 9.0 Hz); 7.11 (s, 1H, CH); 7.33 (d, 2H, 2CH, J = 9.0 Hz); 7.48 (d, 2H, 2CH, J = 9.0 Hz); 7.64 (d, 2H, 2CH, J = 9.0 Hz); 7.67 (d, 2H, 2CH, J = 9.0 Hz); 7.70 (s, 1H, CH); 10.30 (bs, 1H, NH); 11.90 (bs, 1H, NH). ^{13}C NMR (DMSO-d_6, 100 MHz), δ (ppm): 21.42; 41.45 (2C); 52.35 (2C); 103.00; 112.36 (2C); 119.59; 120.31 (2C); 123.06; 126.98; 127.20 (2C); 128.64; 130.17 (2C); 137.07; 137.86; 143.78; 143.92; 148.10; 148.28; 168.79. FAB(+)-MS (m/z, %): 588.2 [(M^++1), 100], 345.1 (16), 247.1 (28), 245.2 (44), 195.1 (20), 190.1 (28), 188.0 (40). *Anal.* Calcd. for $C_{27}H_{27}Cl_2N_5O_2S_2$: C, 55.10; H, 4.62; N, 11.90. Found: C, 55.08; H, 4.64; N, 11.91.

4.1.16. (E)-N-(4-(2-(2-(4-(Bis(2-chloroethyl)amino)benzylidene) hydrazinyl)thiazol-4-yl)phenyl)-4-(trifluoromethyl)-benzenesulfonamide (5e)

N-(4-(2-Chloroacetyl)phenyl)-4-(trifluoromethyl)benzenesulfonamide (**2e**) was reacted with **4**. Yield: 0.20 g, 48%, (dichloromethane/methanol, 90:10, R_f = 0.81); mp 205-207 °C. ^{1}H NMR (DMSO-d_6, 700 MHz), δ (ppm): 3.72–3.79 (m, 8H, 4CH_2); 6.82 (d, 2H, 2CH, J = 9.0 Hz); 7.17 (d, 2H, 2CH, J = 9.0 Hz); 7.18 (s, 1H, CH); 7.51 (d, 2H, 2CH, J = 9.0 Hz); 7.74 (d, 2H, 2CH, J = 9.0 Hz); 7.96 (s, 1H, CH); 7.99 (m, 4H, 4CH); 10.67 (bs, 1H, NH); 11.99 (bs, 1H, NH). ^{13}C NMR (DMSO-d_6, 100 MHz), δ (ppm): 42.49 (2C); 53.38 (2C); 104.36; 113.39 (2C); 121.99 (2C); 124.05; 125.60; 127.14; 128.04 (2C); 128.14 (2C); 129.16 (2C); 129.68 (2C); 131.35; 134.14 (q, J_{C-F} = 32.0 Hz); 138.19; 141.81; 145.19; 149.18; 169.83. FAB(+)-MS (m/z, %): 642.1 [(M^++1), 100], 247.1 (40), 245.2 (68), 195.1 (40), 188.1 (60), 167.1 (12). *Anal.* Calcd. for $C_{27}H_{24}Cl_2F_3N_5O_2S_2$: C, 50.47; H, 3.76; N, 10.90. Found: C, 50.44; H, 3.78; N, 10.92.

4.1.17. (E)-N-(4-(2-(2-(4-(Bis(2-chloroethyl)amino)benzylidene) hydrazinyl)thiazol-4-yl)phenyl)-4-methoxybenzene-sulfonamide (5f)

N-(4-(2-Chloroacetyl)phenyl)-4-methoxybenzenesulfonamide (**2f**) was reacted with **4**. Yield: 0.35 g, 80%, (dichloromethane/methanol, 90:10, R_f = 0.73); mp 198-200 °C with decomp. ^{1}H NMR (DMSO-d_6, 700 MHz), δ (ppm): 3.77 (s, 3H, CH_3); 3.72–3.78 (m, 8H, 4CH_2); 6.79 (d, 2H, 2CH, J = 9.0 Hz); 7.05 (d, 2H, 2CH, J = 9.0 Hz); 7.10 (d, 2H, 2CH, J = 9.0 Hz); 7.12 (s, 1H, CH); 7.48 (d, 2H, 2CH, J = 9.0 Hz); 7.67 (d, 2H, 2CH, J = 9.0 Hz); 7.69 (d, 2H, 2CH, J = 9.0 Hz); 7.91 (s, 1H, CH); 10.23 (bs, 1H, NH); 11.94 (bs, 1H, NH). ^{13}C NMR (DMSO-d_6, 100 MHz), δ (ppm): 41.49 (2C); 52.36 (2C); 56.09; 102.95; 112.26 (2C); 114.86 (2C); 120.24 (2C); 123.00; 127.02 (2C); 128.72 (2C); 129.38 (2C); 129.49; 131.56; 138.10; 144.37; 147.96; 148.19; 162.86; 168.64. FAB(+)-MS (m/z, %): 604.3 [(M^++1), 100], 434.1 (12), 361.0 .920), 247.1 (28), 245.1 (48), 195.1 (24), 190.1 (32), 188.1 (40). *Anal.* Calcd. for $C_{27}H_{27}Cl_2N_5O_3S_2$: C, 53.64; H, 4.50; N, 11.58. Found: C, 53.61; H, 4.53; N, 12.01.

4.1.18. (E)-N-(4-(2-(2-(4-(Bis(2-chloroethyl)amino)benzylidene) hydrazinyl)thiazol-4-yl)phenyl)-4-isopropylbenzene-sulfonamide (5g)

N-(4-(2-Chloroacetyl)phenyl)-4-isopropylbenzenesulfonamide (**2g**) was reacted with **4**. Yield: 0.26 g, 74%, (dichloromethane/methanol, 90:10, R_f = 0.73); mp 199-202 °C with decomp. ^{1}H NMR (DMSO-d_6, 700 MHz), δ (ppm): 1.17 (d, 6H, 2CH_3, J = 7.0 Hz); 2.92 (sept, 1H, CH, J = 7.0 Hz); 3.70–3.78 (m, 8H, 4CH_2); 6.80 (d, 2H, 2CH, J = 9.0 Hz); 7.12 (s, 1H, CH); 7.13 (d, 2H, 2CH, J = 9.0 Hz); 7.42 (d, 2H, 2CH, J = 9.0 Hz); 7.48 (d, 2H, 2CH, J = 9.0 Hz); 7.68 (d, 2H, 2CH,

J = 9.0 Hz); 7.70 (d, 2H, 2CH, J = 9.0 Hz); 7.90 (s, 1H, CH); 10.34 (bs, 1H, NH); 11.88 (bs, 1H, NH). ^{13}C NMR (DMSO-d_6, 100 MHz), δ (ppm): 23.83 (2C); 33.81; 41.53 (2C); 52.39 (2C); 103.03; 112.37 (2C); 119.43; 120.01 (2C); 122.97; 127.07; 127.30 (2C); 127.69 (2C); 128.71; 137.51; 137.57; 138.01; 144.34; 146.19; 147.88; 148.17; 154.11; 168.81. FAB(+)-MS (m/z, %): 616.2 [(M^++1), 100], 373.3 (24), 245.1 (60), 230.1 (16), 209.1 (28), 195.1 (32), 190.1 (52), 188.0 (60), 181.1 (32), 167.0 .916). *Anal.* Calcd. for $C_{29}H_{31}Cl_2N_5O_2S_2$: C, 56.49; H, 5.07; N, 11.36. Found: C, 56.51; H, 5.04; N, 11.39.

4.1.19. (E)-N-(4-(2-(2-(4-(Bis(2-chloroethyl)amino)benzylidene) hydrazinyl)thiazol-4-yl)phenyl)-4-tert-butylbenzene-sulfonamide (5 h)

4-*tert*-Butyl-*N*-(4-(2-chloroacetyl)phenyl)benzenesulfonamide (**2h**) was reacted with **4**. Yield: 0.33 g, 97%, (dichloromethane/methanol, 90:10, R_f = 0.74); mp 210-212 °C with decomp. ^{1}H NMR (DMSO-d_6, 700 MHz), δ (ppm): 1.24 (s, 9H, $3CH_3$); 3.72–3.78 (m, 8H, $4CH_2$); 6.80 (d, 2H, 2CH, J = 9.0 Hz); 7.12 (s, 1H, CH); 7.14 (d, 2H, 2CH, J = 9.0 Hz); 7.48 (d, 2H, 2CH, J = 9.0 Hz); 7.57 (d, 2H, 2CH, J = 9.0 Hz); 7.68 (d, 2H, 2CH, J = 9.0 Hz); 7.71 (d, 2H, 2CH, J = 9.0 Hz); 7.90 (s, 1H, CH); 10.37 (bs, 1H, NH); 11.89 (bs, 1H, NH). ^{13}C NMR (DMSO-d_6, 100 MHz), δ (ppm): 31.18 (3C); 35.32; 41.48 (2C); 52.36 (2C); 103.01; 112.35 (2C); 119.38; 119.92 (2C); 122.98; 126.63 (2C); 127.03 (2C); 127.07 (2C); 128.71; 137.23; 137.31; 138.02; 138.47; 144.30; 148.16; 156.45; 168.75. FAB(+)-MS (m/z, %): 630.3 [(M^++1), 100], 387.3 (28), 245.1 (80), 195.1 (40), 190.1 (64), 188.0 (88), 181.1 (20), 167.0 (16), 133.1 (16). *Anal.* Calcd. for $C_{30}H_{33}Cl_2N_5O_2S_2$: C, 57.13; H, 5.27; N, 11.10. Found: C, 57.15; H, 5.25; N, 11.12.

4.1.20. ((E)-N-(4-(2-(2-(4-(Bis(2-chloroethyl)amino)benzylidene) hydrazinyl)thiazol-4-yl)phenyl)-2,3,4,5,6-pentafluoro-benzenesulfonamide (5i)

N-(4-(2-Chloroacetyl)phenyl)-2,3,4,5,6-pentafluorobenzenesulfonamide (**2i**) was reacted with **4**. Yield: 0.24 g, 73%, (dichloromethane/methanol, 90:10, R_f = 0.75); mp > 260 °C. ^{1}H NMR (DMSO-d_6, 700 MHz), δ (ppm): 3.72–3.80 (m, 8H, $4CH_2$); 6.80 (d, 2H, 2CH, J = 9.0 Hz); 7.19 (d, 2H, 2CH, J = 9.0 Hz); 7.20 (s, 1H, CH); 7.48 (d, 2H, 2CH, J = 9.0 Hz); 7.78 (d, 2H, 2CH, J = 9.0 Hz); 7.90 (s, 1H, CH); 11.36 (bs, 1H, NH); 11.89 (bs, 1H, NH). ^{13}C NMR (DMSO-d_6, 100 MHz), δ (ppm): 41.48 (2C); 52.35 (2C); 103.61; 112.35 (2C); 115.28 (m); 121.06 (2C); 123.11; 127.21 (2C); 128.59 (2C); 131.38; 135.81; 136.77 (m); 139.28 (m); 142.88 (m); 143.24 (m); 143.66; 145.75 (m); 148.06; 148.56; 168.85. FAB(+)-MS (m/z, %): 664.1 [(M^++1), 100], 421.1 (28), 245.1 (80), 195.1 (64), 181.0 (68), 167.0 (32), 145.0 (28). *Anal.* Calcd. for $C_{26}H_{20}Cl_2F_5N_5O_2S_2$: C, 46.99; H, 3.03; N, 10.54. Found: C, 47.01; H, 3.00; N, 10.57.

4.1.21. (E)-N-(4-(2-(2-(4-(Bis(2-chloroethyl)amino)benzylidene) hydrazinyl)thiazol-4-yl)phenyl)-5-(dimethylamino)-naphthalene-1-sulfonamide (5j)

N-(4-(2-Chloroacetyl)phenyl)-5-(dimethylamino)naphthalene-1-sulfonamide (**2j**) was reacted with **4**. Yield: 0.21 g, 64%, (dichloromethane/methanol, 90:10, R_f = 0.79); mp 180 °C with decomp. ^{1}H NMR (DMSO-d_6, 700 MHz), δ (ppm): 2.79–2.87 (s, 6H, $2CH_3$); 3.72–3.78 (m, 8H, $4CH_2$); 6.79 (d, 2H, 2CH, J = 9.0 Hz); 7.04–7.07 (m, 3H, 3CH); 7.26–7.36 (m, 1H, CH); 7.46 (d, 2H, 2CH, J = 9.0 Hz); 7.60 (d, 2H, 2CH, J = 9.0 Hz); 7.60–7.66 (m, 2H, 2CH); 7.88 (s, 1H, CH); 8.23 (s, 1H, CH); 8.38–8.50 (m, 2H, 2CH); 10.78 (bs, 1H, NH); 11.84 (bs, 1H, NH). ^{13}C NMR (DMSO-d_6, 100 MHz), δ (ppm): 41.49 (2C); 46.11 (2C); 52.36 (2C); 102.83; 112.35 (2C); 117.88; 118.68; 119.26 (2C); 122.20; 123.10; 125.06; 126.98 (2C); 128.17; 128.59 (2C); 129.25; 129.73; 129.84; 130.69; 135.57; 137.46; 143.65; 148.05; 168.76. FAB(+)-MS (m/z, %): 667.3 [(M^++1), 100], 247.1 (32), 245.1 (56), 241.2 (32), 195.1 (32), 190.0 (52), 185.1 (64), 170.1 (64), 168.0 (48), 149.1 (32), 117.0 (20). *Anal.* Calcd. for $C_{32}H_{32}Cl_2N_6O_2S_2$: C, 57.56; H, 4.83; N, 12.59. Found: C, 57.59; H, 4.84; N, 12.60.

4.2. Biological activity

4.2.1. Cells

Biphenotypic B myelomonocytic leukemia MV4-11, human lung carcinoma A549, human breast carcinoma MCF-7, human colon carcinoma HCT116 and normal mouse fibroblast BALB/3T3 cells were obtained from American Type Culture Collection (Rockville, Maryland, USA). All the cell lines are being maintained at the Institute of Immunology and Experimental Therapy, Wroclaw, Poland.

MV4-11 cells were cultured in RPMI 1640 medium (Gibco, UK) with 2 mM L-glutamine adjusted to contain 1.0 mM sodium pyruvate, and 10% fetal bovine serum (FBS) (all from Sigma–Aldrich, Germany). A549 and HCT116 cells were cultured in RPMI 1640+Opti-MEM (1:1) (both from Gibco, UK), MCF-7 cells in Eagle medium (IIET, Wroclaw, Poland), BALB/3T3 in Dulbecco medium (IIET, Poland) supplemented with 2 mM L-glutamine and 1.0 mM sodium pyruvate, 10% fetal bovine serum (all from Sigma-Aldrich, Germany).

The MCF-7 cell culture was supplemented with 0.8 mg/L of insulin (Sigma-Aldrich, Germany). All culture media were supplemented with 100 units/ml penicillin, and 100 μg/ml streptomycin (both from Polfa Tarchomin S.A., Poland). All cell lines were grown at 37 °C with 5% CO_2 humidified atmosphere.

4.2.2. Compounds

Prior to usage, the compounds were dissolved in DMSO and culture medium (1: 9) to the concentration of 1 mg/ml, and subsequently diluted in culture medium to reach the required concentrations (0.1, 1, 10 and 100 μg/ml).

4.2.3. In vitro antiproliferative assay

Twenty four hours prior to the addition of the tested compounds, the cells counted using Burker hemocytometer were plated in 96-well plates (Sarstedt, Germany) at a density of 1×10^4 cells per well or 0.5×10^4 of the HCT116 cells. The assay was performed after 72 h of exposure to varying concentrations of the tested agents [29,30]. The *in vitro* cytotoxic effect of all agents was examined using the SRB assay for adherent cells (A549, MCF-7, HCT116, BALB/3T3) or MTT assay for leukaemia cells (MV4-11) as described previously. The results were calculated as an IC_{50} (inhibitory concentration 50) – the concentration of tested agent which inhibits proliferation of 50% of the cancer cell population. IC values were calculated for each experiment separately and mean values ± SD are presented in the Table 1. Each compound in each concentration was tested in triplicate in a single experiment, which was repeated 3-7 times.

4.2.4. SRB cytotoxic test

Cells were attached to the bottom of plastic wells by fixing them with cold 50% TCA (trichloroacetic acid, POCH, Gliwice, Poland) on top of the culture medium in each well. The plates were incubated at 4 °C for 1 h and then washed five times with tap water. The cellular material fixed with TCA was stained with 0.14% sulforhodamine B (SRB, Sigma-Aldrich, Germany) and dissolved in 1% acetic acid (POCH, Gliwice, Poland) for 30 min. Unbound dye was removed by rinsing (4X) in 1% acetic acid. The protein-bound dye was extracted with 10 mM unbuffered Tris base (Sigma-Aldrich Chemie GmbH, Steinheim, Germany) for determination of the optical density (λ = 540 nm) in a computer-interfaced, 96-well Synergy H4 (BioTek Instruments USA) photometer microtiter plate

reader [31].

4.2.5. MTT cytotoxic test

Twenty microliter of MTT solution (MTT: 3-(4,5-dimethylthiazol-2-yl)-2,5-diphenyl tetrazolium bromide, stock solution: 5 mg/ml) was added to each well and incubated for 4 h. After the incubation time was complete, 80 μl of the lysis mixture was added to each well (lysis mixture: 225 ml dimethylformamide, 67.5 g sodium dodecyl sulfate and 275 ml of distilled water). The optical densities of the samples were read after 24 h on a Synergy H4 (BioTek Instruments USA) photometer microtiter plate reader at 570 nm. All of chemicals were obtained from Sigma-Aldrich, Germany [31].

4.2.6. Cellular staining and colocalization

To visualize the accumulation of the compound **5j** within the cells, 10×10^3 HCT116 cells in a 300 μL growth medium were plated into an 8-well LabTek chambered cover glass (Nunc) and incubated under standard conditions at 37 °C in a humidified atmosphere at 5% CO_2 for 24 h. After this, the cells were treated with the compound **5j** being tested at a concentration of 16 μg/ml and incubated for a further 2 h. After incubation the cells were treated with cellular Trackers: ER-Tracker™ (Molecular Probes) concentration 100 nM for 1 h, MitoTracker® Orange (Molecular Probes) concentration 1 μM for 0.5 h, and Hoechst (Thermo Fisher Scientific) concentration 6.5 μM for 1 h. After incubation with the appropriate dyes the cells were washed three times with PBS and then 300 μL of PBS was added. Observation of the cells was carried out using an Olympus Fluoview FV1000 confocal laser scanning system equipped with the Olympus IX81 inverted microscope (Olympus, Poland) immediately after staining. Images acquisition was performed using a 60x oil immersion objective lens. Analysis and processing images were performed using an ImageJ 1.41 (Wayne Rasband, National Institutes of Health, USA).

4.3. Spectroscopy

The absorption and fluorescence spectra were measured at room temperature in a 10 mm quartz cell with a U-2900 spectrophotometer (Hitachi) and an F-7000 spectrofluorimeter (Hitachi), respectively. The stock solutions (10 mM) that had been prepared in DMSO were further diluted to working concentrations starting from 0.1 mM. The fluorescence quantum yields were measured using the comparative method with anthracene in cyclohexane as a reference ($\Phi_{Ref} = 0.34$). We prepared standard and test solutions of decreasing concentrations in order to provide absorbance in the range of 0.1 to 0.01 at the excitation wavelength. The fluorescence spectra of all of the solutions were measured at room temperature in a 10 mmcell using an F-7000 spectrofluorimeter (Hitachi). The fluorescence quantum yields of the dyes that were tested were calculated as follows:

$$\phi = \phi_{Ref}\left(\alpha_{Dye}/\alpha_{Ref}\right)\left(\eta^2_{Dye}/\eta^2_{Ref}\right)$$

where subscripts *Dye* and *Ref* indicate test and standard samples, respectively, Φ is the fluorescence quantum yield, α is the gradient obtained from the plot integrated fluorescence intensity versus absorbance and η is the refractive index of solvents that were applied.

4.4. Quantum mechanical calculations

Spectroscopic properties have been calculated within DFT and TD-DFT approximations using the Gaussian 09 software package [32] with the B3LYP exchange-correlation functional [33] and 6-31 + G(d,p) basis set. The effects of the solvent were evaluated using the PCM model [33–35] in which a cavity is created via a series of overlapping spheres [36] with standard dielectric constants (ε) of 46.826 for DMSO. Electronic absorption transition energies for 50 spin-allowed singlet–singlet and fluorescence emission spectra made of the 4 spin-allowed transitions were considered using the external iteration (EI) approach. The molecular electron densities for each derivative were determined from the wave functions using the CUBE option implemented in Gaussian 09 and visualized using GaussView 5.0. The molecular energy levels were analyzed using Chemissian software [32].

Geometrical parameters of the investigated complexes were optimized using the DFT with the B3LYP functional and the 6-311G** basis set. Vibrational frequencies were evaluated within the same approximation to confirm that the resulting structures correspond to real minima on potential energy surface. Next, interaction and binding energies were calculated using the supermolecular approach and counterpoise-correcting the results. On the basis of the conclusions of our recent work [13] the DFT/M06-2X approximation and the 6-311++G** basis set were chosen for that purpose. All calculations were carried out using the Gaussian 09 program [32].

4.5. Automated docking setup

Flexible docking was performed by means of the FlexX program [37] as implemented in LeadIT software package [38]. Model of the Topo I binding site on the structure deposited in the Protein Data Bank [39] under the PDB ID 1SEU [40] and model of the Topo II binding site under the PDB ID 3QX3 [41] were employed. The native ligands within the active sites, the camptothecin and the etoposide (anticancer drug), respectively, were removed. In the case of docking simulation within Topo II binding site, two water molecules (HOH-1376-A and HOH-1461-A) were allowed. The active sites were defined to include all atoms within 6.5 Å radius of the native ligands. The first 100 top ranked docking poses were saved for each docking run. For all compounds their protonated forms were considered, as recommended by FlexX program.

Conflict of interest

The authors confirm that this article content has no conflicts of interest.

Acknowledgements

This study was supported by the Nicolaus Copernicus University (grant No. 01/CM/2014). We thank Centro de Supercomputación de Galicia (CESGA) and Wrocław Centre for Networking and Supercomputing, WCSS, Wrocław, Poland, http://www.wcss.wroc.pl, Grant no. 18. for computational resources.

Appendix A. Supplementary data

Supplementary data related to this article can be found at http://dx.doi.org/10.1016/j.molstruc.2016.04.058.

References

[1] P. Boyle, B. Levin, World cancer Report, International Agency for Research on Cancer, Lyon, 2008. Reference available from, http://www.iarc.fr/en/publications/pdfs.online/wcr/2008/wcr_2008.pdf.
[2] J.S.I. Ferlay, M. Ervik, R. Dikshit, S. Eser, C. Mathers, M. Rebelo, D.M. Parkin, D. Forman, F. Bray, Cancer Incidence and Mortality Worldwide: IARC CancerBase No. 11 [Internet]; GLOBOCAN 2012 v1.0 2013, International Agency

for Research on Cancer, Lyon, France, 2013.
[3] S. Puyo, D. Montaudon, P. Pourquier, From old alkylating agents to new minor groove binders, Crit. Rev. Oncol. Hematol. 89 (2014) 43–61.
[4] K. Suzukake, B.P. Vistica, D.T. Vistica, Dechlorination of L-phenylalanine mustard by sensitive and resistant tumor cells and its relationship to intracellular glutathione content, Biochem. Pharmacol. 32 (1983) 165–167.
[5] J.M. Kaldor, N.E. Day, K. Hemminki, Quantifying the carcinogenicity of antineoplastic drugs, Eur. J. Cancer Clin. Oncol. 24 (1988) 703–711.
[6] M.R. Osborne, P.D. Lawley, C. Crofton-Sleigh, W. Warren, Products from alkylation of DNA in cells by melphalan: human soft tissue sarcoma cell line RD and Escherichia coli WP2, Chem. Biol. Interact. 97 (1995) 287–296.
[7] R. Saffhill, G.P. Margison, P.J. O'Connor, Mechanisms of carcinogenesis induced by alkylating agents, Biochim. Biophys. Acta. 823 (1985) 111–145.
[8] B.J. Sanderson, A.J. Shield, Mutagenic damage to mammalian cells by therapeutic alkylating agents, Mutat. Res. 355 (1996) 41–57.
[9] Y.-D. Wang, J. Dziegielewski, N.R. Wurtz, B. Dziegielewska, P.B. Dervan, T.A. Beerman, DNA crosslinking and biological activity of a hairpin polyamide-chlorambucil conjugate, Nucleic Acids Res. 31 (2003) 1208–1215.
[10] T.A. Gourdie, K.K. Valu, G.L. Gravatt, T.J. Boritzki, B.C. Baguley, L.P. Wakelin, W.R. Wilson, P.D. Woodgate, W.A. Denny, DNA-directed alkylating agents. 1. Structure-activity relationships for acridine-linked aniline mustards: consequences of varying the reactivity of the mustard, J. Med. Chem. 33 (1990) 1177–1186.
[11] S. McClean, C. Costelloe, W.A. Denny, M. Searcey, L.P. Wakelin, Sequence selectivity, cross-linking efficiency and cytotoxicity of DNA-targeted 4-anilinoquinoline aniline mustards, Anticancer Drug Des. 14 (1999) 187–204.
[12] G. Pezzoni, M. Grandi, G. Biasoli, L. Capolongo, D. Ballinari, F.C. Giuliani, B. Barbieri, A. Pastori, E. Pesenti, N. Mongelli, Biological profile of FCE 24517, a novel benzoyl mustard analogue of distamycin A, Br. J. Cancer 64 (1991) 1047–1050.
[13] K.Z. Łączkowski, K. Misiura, M. Świtalska, J. Wietrzyk, A. Baranowska-Łączkowska, B. Fernández, A. Paneth, T. Plech, Synthesis and *in vitro* antiproliferative activity of thiazole-based nitrogen mustards. The hydrogen bonding interaction between model systems and nucleobases, Anti Cancer Agents Med. Chem. 14 (2014) 1271–1281.
[14] K.Z. Łączkowski, K. Motylewska, A. Baranowska-Łączkowska, A. Biernasiuk, K. Misiura, A. Malm, B. Fernández, Synthesis, antimicrobial evaluation and theoretical prediction of NMR chemical shifts of thiazole and selenazole derivatives with high antifungal activity against *Candida* spp, J. Mol. Struct. 1108 (2016) 427–437.
[15] K.Z. Łączkowski, K. Misiura, A. Biernasiuk, A. Malm, Discovery and evaluation of efficient selenazoles with high antifungal activity against *Candida* spp, Med. Chem. 11 (2015) 118–127.
[16] K.Z. Łączkowski, K. Misiura, A. Biernasiuk, A. Malm, A. Siwek, T. Plech, E. Ciok-Pater, K. Skowron, E. Gospodarek, Synthesis, in vitro biological screening and molecular docking studies of novel camphor-based thiazoles, Med. Chem. 10 (2014) 600–608.
[17] K.Z. Łączkowski, K. Misiura, A. Biernasiuk, A. Malm, A. Siwek, T. Plech, Synthesis, antimicrobial activities and molecular docking studies of novel 6-hydroxybenzofuran-3(2*H*)-one based 2,4-disubstituted 1,3-thiazoles, Lett. Drug Des. Discov. 10 (2013) 798–807.
[18] J. Karthikeyan, P. Parameshwara, A. Nityananda Shetty, Analytical properties of *p*-[*N*,*N*-bis(2-chloroethyl)amino]-benzaldehydethiosemicarbazone: spectrophotometric determination of palladium(II) in alloys, catalysts, and complexes, Environ. Monit. Assess. 173 (2011) 569–577.
[19] R.I. Geran, N.H. Greenberg, M.M. MacDonald, A.M. Schumacher, B.D. Abbott, Protocols for screening chemical agents and natural products against animal tumors and other biological systems, Cancer Chemother. Rep. Part 3 3 (1972) 59–61.
[20] K. Sugano, M. Kansy, P. Artursson, A. Avdeef, S. Bendels, L. Di, G.F. Ecker, B. Faller, H. Fischer, G. Gerebtzoff, H. Lennernaes, F. Senner, Nat. Rev. Drug Discov. 9 (2010) 597–614.
[21] C. Adamo, D. Jacquemin, The calculations of excited-state properties with time-dependent density functional theory, Chem. Soc. Rev. 42 (2013) 845–856.
[22] Y. Chen, J. Zhao, H. Guo, L. Xie, Geometry relaxation-induced large stokes shift in red-emitting borondipyrro-methenes (BODIPY) and applications in fluorescent thiol probes, J. Org. Chem. 77 (2012) 2192–2206.
[23] B. Valeur, Molecular Fluorescence: Principles and Applications, Wiley-VCH Verlag, Weinheim, 2001.
[24] M. Rams-Baron, M. Dulski, A. Mrozek-Wilczkiewicz, M. Korzec, W. Cieslik, E. Spaczyńska, P. Bartczak, A. Ratuszna, J. Polanski, R. Musioł, Synthesis of new styrylquinoline cellular dyes, fluorescent properties, cellular localization and cytotoxic behavior, PLoS One 10 (2015) e0131210.
[25] J. Kornhuber, A.W. Henkel, T.W. Groemer, S. Städtler, O. Welzel, P. Tripal, A. Rotter, S. Bleich, S. Trapp, Lipophilic cationic drugs increase the permeability of lysosomal membranes in a cell culture system, J. Cell Physiol. 224 (2010) 152–164.
[26] Y.-C. Chang, J.D. Wang, K.K. Svoboda, R.P. Casillas, J.D. Laskin, M.K. Gordon, D.R. Gerecke, Sulfur mustard induces an endoplasmic reticulum stress response in the mouse ear vesicant model, Toxicol. Appl. Pharmacol. 268 (2013) 178–187.
[27] A. Polavarapu, J.A. Stillabower, S.G.W. Stubblefield, W.M. Taylor, M.-U. Baik, The mechanism of guanine alkylation by nitrogen mustards: a computational study, J. Org. Chem. 77 (2012) 5914–5921.
[28] J.L. Nitiss, Targeting DNA topoisomerase II in cancer chemotherapy, Nat. Rev. Cancer 9 (2009) 338–350.
[29] J. Bramson, A. McQuillan, R. Aubin, M. Alaoui-Jamali, G. Batist, G. Christodoulopoulos, L.C. Panasci, Nitrogen mustard drug resistant B-cell chronic lymphocytic leukemia as an in vivo model for crosslinking agent resistance, Mut. Res. 336 (1995) 269–278.
[30] K. Sidoryk, M. Świtalska, J. Wietrzyk, A. Jaromin, M. Piętka-Ottlik, P. Cmoch, J. Zagrodzka, W. Szczepek, L. Kaczmarek, W. Peczyńska-Czoch, Synthesis and biological evaluation of new amino acid and dipeptide derivatives of neocryptolepine as anticancer agents, J. Med. Chem. 55 (2012) 5077–5087.
[31] L.V. Rubinstein, R.H. Shoemaker, K.D. Paul, R.M. Simon, S. Tosini, P. Skehan, D.A. Sudiero, A. Monks, M.R. Boyd, Comparison of in vitro anticancer-drug-screening data generated with a tetrazolium assay versus a protein assay against a diverse panel of human tumor cell lines, J. Nat. Cancer Inst. 82 (1990) 1113–1118.
[32] M.J. Frisch, G.W. Trucks, H.B. Schlegel, G.E. Scuseria, M.A. Robb, J.R. Cheeseman, G. Scalmani, V. Barone, B. Mennucci, G.A. Petersson, H. Nakatsuji, M. Caricato, X. Li, H.P. Hratchian, A.F. Izmaylov, J. Bloino, G. Zheng, J.L. Sonnenberg, M. Hada, M. Ehara, K. Toyota, R. Fukuda, J. Hasegawa, M. Ishida, T. Nakajima, Y. Honda, O. Kitao, H. Nakai, T. Vreven, J.A. Montgomery, J.E. Peralta, F. Ogliaro, M. Bearpark, J.J. Heyd, E. Brothers, K.N. Kudin, V.N. Staroverov, R. Kobayashi, J. Normand, K. Raghavachari, A. Rendell, J.C. Burant, S.S. Iyengar, J. Tomasi, M. Cossi, N. Rega, N.J. Millam, M. Klene, J.E. Knox, J.B. Cross, V. Bakken, C. Adamo, J. Jaramillo, R. Gomperts, R.E. Stratmann, O. Yazyev, A.J. Austin, R. Cammi, C. Pomelli, J.W. Ochterski, R.L. Martin, K. Morokuma, V.G. Zakrzewski, G.A. Voth, P. Salvador, J.J. Dannenberg, S. Dapprich, A.D. Daniels, Ö. Farkas, J.B. Foresman, J.V. Ortiz, J. Cioslowski, D.J. Fox, Gaussian 09, Revision C.01, A.02, Gaussian, Inc., Wallingford, 2009.
[33] M. Cossi, V. Barone, R. Cammi, J. Tomasi, *Ab initio* study of solvated molecules: a new implementation of the polarizable continuum model, Chem. Phys. Lett. 255 (1996) 327–335.
[34] J.B. Foresman, T.A. Keith, K.B. Wiberg, J. Snoonian, M.J. Frisch, Solvent effects. 5. Influence of cavity shape, truncation of electrostatics and electron correlation on ab initio reaction field calculations, J. Phys. Chem. 100 (1996) 16098–16104.
[35] J. Tomasi, B. Mennucci, R. Cammi, Quantum mechanical continuum solvation models, Chem. Rev. 105 (2005) 2999–3093.
[36] J. Tomasi, B. Mennucci, E. Cancès, The IEF version of the PCM solvation method: an overview of a new method addressed to study molecular solutes at the QM *ab initio* level, J. Mol. Struct. Theochem. 464 (1999) 211–226.
[37] B. Kramer, M. Rarey, T. Lengauer, Evaluation of the FlexX incremental construction algorithm for protein-ligand docking, Proteins 37 (1999) 228–241.
[38] LeadIT 2.1.0, BioSolveIT, GmbH, St. Augustin, Germany, 2012.
[39] G. Gilliland, T.N. Bhat, H. Weissig, I.N. Shindyalov, P.E. Bourne, The protein data bank, Nucleic Acids Res. 28 (2000) 235–242.
[40] B.L. Staker, M.D. Feese, M. Cushman, Y. Pommier, D. Zembower, L. Stewart, A.B. Burgin, Structures of three classes of anticancer agents bound to the human topoisomerase I-DNA covalent complex, J. Med. Chem. 48 (2005) 2336–2345.
[41] C.C. Wu, T.K. Li, L. Farh, L.Y. Lin, T.S. Lin, Y.J. Yu, T.J. Yen, C.W. Chiang, N.L. Chan, Structural basis of type II topoisomerase inhibition by the anticancer drug etoposide, Science 333 (2011) 459–462.